Heliyon 6 (2020) e03735

Contents lists available at ScienceDirect

Heliyon

journal homepage: www.cell.com/heliyon

Research article

Effects of palm biodiesel and blends of biodiesel with organic acids on metals

L.M. Baena [a,*], J.A. Calderón [b]

[a] Grupo de Calidad, Metrología y Producción, Instituto Tecnológico Metropolitano ITM, Medellín, Colombia
[b] Centro de Investigación, Innovación y Desarrollo de Materiales-CIDEMAT, Universidad de Antioquia, Medellín, Colombia

ARTICLE INFO

Keywords:
Materials science
Materials chemistry
Corrosion
Biodiesel
Corrosion inhibitor
Fatty acid
Metallic material

ABSTRACT

This paper presents the corrosion behavior studies of five metallic materials used in auto part manufacturing exposed to pure palm biodiesel (B100) and palm biodiesel mixed with acidic species commonly found in biodiesel. Samples of AISI-SAE 1005 carbon steel, AISI-SAE 304 stainless steel, tin, aluminum and copper were exposed to a temperature of 45 °C for 12 months. The highest corrosion rates were present in totally immersed copper (B100-acetic acid blend) and in carbon steel (B100-oleic acid blend). The most corrosive blends for the metallic materials were B100-linoleic acid, B100-oleic acid and B100-acetic acid. The efficacy of two corrosion inhibitors, ethylenediamine (EDA) and tert-butylamine (TBA) increased as a function of exposure time. The characterization tests allowed the detection of different species, in the products of steel corrosion, associated with, lepidocrocite, ferrihydrite, magnetite, and some iron carbonates. In turn, cuprite, malachite, azurite, and some copper carbonates were found on the copper samples. Such corrosion products formed protective layers on the surface of the metals, which is reflected in a decrease in corrosion rates over time.

1. Introduction

From the point of view of compatibility, biodiesel is a highly aggressive fuel with metallic materials because of its composition and how easily it undergoes oxidation reactions during its usage and storage. As biodiesel degrades, its corrosive and harmful character increases for materials that comprise automotive systems and are in direct contact with it [1]. The oxidation reactions of biodiesel generate a large number of products, such as aldehydes, ketones, water, alcohols, and carboxylic acids, among others [2]. The oxidation process of biodiesel consists in the formation of hydroperoxides (ROOH) from free radical reactions, which lead to the generation of carboxylic acids that contain between 1 and 11 carbon atoms, such as acetic acid, formic acid, propionic acid, and fatty acids [2]. The presence of those products in biodiesel increases its total acidity and, therefore, the risk of corrosion in the vehicle system [3]. Biodiesel has a tendency to absorb water from the environment, approximately 30 times more than traditional diesel [4]; for that reason, the humidity limit established in standards regulating the quality of biodiesel is 500ppm [5].

The water present in biodiesel is transformed into water vapor as a result of the temperature increase; then, it condenses on the surface of metal auto parts, which can cause corrosion [6]. The water contained in biodiesel can also generate hydrolytic reactions, which lead to the formation of organic acids [7]. Aquino et al [8] characterized the degradation of biodiesel through oxidation stability, viscosity change, and water content increase. Said authors observed an increase in water content in biodiesel at 55 °C after the immersion of copper and brass. Their results revealed that corrosion caused by biodiesel is not associated with the formation of free or absorbed water because the lowest thickness losses in the immersed metals were obtained under the condition that led to the highest water content (5 days of immersion). Biodiesel quality can be affected by the presence of microorganisms during storage, which influences the corrosion deterioration of metallic tanks, since biodiesel is more prone to microbial contamination than diesel [9]. Such microbial contamination of biodiesel is mainly attributed to its hygroscopic nature because the presence of water produces a phase separation between water and biodiesel, which allows the formation of a microbial film at the water-biodiesel interface [10]. The presence of 1% of water in biodiesel has been reported to be sufficient for the formation of biofilms from microorganisms, fungi, and yeasts at the oil-water interface [11]. Some of the yeasts and fungi most commonly found in biofilms formed in fuels are Candida,

* Corresponding author.
E-mail address: libiabaena@itm.edu.co (L.M. Baena).

https://doi.org/10.1016/j.heliyon.2020.e03735
Received 8 August 2018; Received in revised form 9 September 2019; Accepted 31 March 2020

Rhodotorula, Aspergillus, Paecilomyces, Fusarium, Hormoconis, Penicillium, and Alternaria [11]. The corrosion behavior of different metals (such as copper, brass, bronze, aluminum, cast iron, and carbon steel) exposed to various types of biodiesel has been studied by several researchers because said materials are used to make auto parts that are in direct contact with the fuel [1], generally, the tank, pump, fuel filters, and injectors [7]. However, it has not yet been reported if the corrosion rates produced by biodiesel lie within the acceptable limits of auto parts [7]. Another study delved into the corrosion of biodiesel from different sources (such as Jatropha Curcas, Karanja, Mahua and Salvadora seeds) on aluminum pistons [12]. Chew et al [13] investigated the corrosion behavior of palm biodiesel on aluminum and magnesium by means of immersion tests at room temperature; they observed a higher corrosion rate of magnesium compared to aluminum.

Enzhu et al [14] carried out immersion tests on biodiesel and diesel at 43 °C to evaluate aluminum, carbon steel, stainless steel, and copper. In their work, copper and carbon steel showed the highest corrosion rates. Moreover, the mechanisms of corrosion of metallic materials were mainly due to the chemical reactions produced in biodiesel. In another work, ASTM 1045 steel was evaluated in contact with palm biodiesel and pure diesel by immersion tests at 27, 50, and 80 °C for 30, 60, and 120 days; in that case, biodiesel exhibited corrosion deterioration [6].

Geller et al [15] observed that copper and its alloys showed greater corrosion damage than 316 stainless steel and carbon steel exposed to biodiesel obtained from bird fat biodiesel. Sgroi et al [16] investigated the effects of biodiesel on copper alloys. They found pitting corrosion on filter components made from copper alloys and, thus, contamination of biodiesel with released copper ions. Norouzi et al [10] studied the corrosion of aluminum and copper caused by blends of diesel with rapeseed biodiesel in concentrations of 0, 50, 75, and 100% at 80 °C for 600 h. Said authors observed that corrosion deterioration increased along with the concentration of biodiesel. They also found that copper is more susceptible to corrosion than aluminum in all exposure means. Cursaru et al [11] evaluated aluminum, copper, and carbon steel in pure sunflower biodiesel (B100), biodiesel mixed with 80% diesel (B20), and traditional diesel (B0) at room temperature and 60 °C for 3000 h. Sunflower biodiesel was observed to be more corrosive than diesel, and metal corrosion and fuel degradation depended on temperature. Additionally, copper was the most prone to corrosion in biodiesel compared to carbon steel and aluminum. In general, copper alloys are more prone to corrosion than ferrous and aluminum alloys [7]. Fazal et al. [17] investigated the corrosion behavior of a type of carbon steel in B0 (diesel), B50 (50% biodiesel in diesel), and B100 (pure biodiesel) at room temperature, 50 and 80 °C, by means of static immersion tests conducted for 1200 h. Such researchers observed that the corrosion deterioration of the exposed metal specimens increased along with the temperature of the fuels and that the content of water and products generated from the oxidation reactions grew at high temperatures. In another study Fazal et al. [18] investigated the stability of palm biodiesel and its chemical composition after exposing it to copper and carbon steel samples at room temperature for 20, 40, and 60 days. They observed that copper significantly affects the stability of some biodiesel properties such as viscosity, water content, calorific value, and density, among others. Nevertheless, corrosion research into blends of biodiesel with fatty and organic acids has not been reported thus far.

Therefore, this paper presents a study into the corrosion of metals commonly used in auto part manufacturing exposed to palm biodiesel and blends of biodiesel with fatty and organic acids by immersion tests at different temperatures and exposure times. Such corrosion in biodiesel-acid blends is evaluated because said acidic species can be produced by hydrolytic and oxidation reactions of the fuel, leading, in principle, to greater corrosiveness in the system, which should be analyzed in depth.

2. Experimental methodology

2.1. Materials

The corrosion behavior of AISI-SAE 304 stainless steel (SS), low carbon steel (ASTM 1005; contains 0.013% C, 0,088% Mn, 0,045% Si, 0,012% P máx, 0,009% S max and 99,542% Fe) (CS), 99% electrolytic tin (Sn), 99% electrolytic copper (Cu), and 99% electrolytic aluminum (Al) was investigated by means of a static immersion test. The metal specimens under study were prepared according to the procedures described in ASTM G1-90 [19]. Square corrosion coupons 0.2 cm thick with an area of 2 cm^2 and a hole of 0.02 cm^2 each were used.

2.2. Immersion test

This test was prepared according to the procedures described in described in ASTM G31-72 [20] and SAE J1747 [21]. Exposure of the metals was performed in triplicate in glass containers (5-liter capacity) with 2.5 l of test fuel. The specimens were in contact with the fuel under 3 exposure conditions: (1) total immersion; (2) partial immersion, i.e., half liquid-half vapor; and (3) in the vapor phase. The glass containers with the test fuels and the metal samples were placed in a water bath at room temperature and at 45 °C. The exposure times were 3, 6, and 12 months.

2.3. Test fuels

The biodiesel used in this work to evaluate metal corrosion was obtained from a basic transesterification reaction between palm oil and methanol employing KOH as a catalyst. Gas Chromatography (GC) was implemented for the chemical characterization (methyl ester composition) of biodiesel (see Table 1). Such test was performed in accordance with EN 14103, on an Agilent 7890A capillary column gas chromatograph Agilent J & W HP-INNOWax, a flame ionization detector, and tetradecanoic acid as the internal standard. The content of methyl esters in the pure biodiesel (B100) is approximately 97% (mass/mass); the water amount content in biodiesel, 0.14%; and the composition of saturated and monounsaturated esters, 43.3% (C16:0) and 41.8% (C18:1), respectively. The physicochemical properties of the palm biodiesel used in this study are shown in Table 2. In order to evaluate the effect of the organic acids on the metallic materials in contact with the biodiesel, four binary blends of B100 and acids were produced. The organic compounds added to the biodiesel were myristic, palmitic, oleic, linoleic, stearic and acetic acids. The B100-acetic acid blend was evaluated because said acid is one of the most aggressive acidic species for metallic materials and it is commonly formed as a result of oxidation reactions. Table 3 shows the physical and chemical characteristics of all acids compunds used in the blends employed in this work. The ASTM D6751 standard indicates that the maximum acid concentration allowed in biodiesel must be 0.8 mg KOH/g and that this value is equivalent to 0.32% acid. The total acid number (TAN) is expressed in milligrams (mg) of potassium hydroxide required to neutralize one gram of acid present in biodiesel, thus determining the level of free fatty acids generated in the production of biodiesel or from oxidation reactions [22]. Therefore, the biodiesel was mixed with 0.32% of acids in order to increase the aggressiveness of the test fuels.

2.4. Evaluation of the effect of corrosion inhibitors

Fuel blends were produced with oleic, linoleic, and acetic acids as well as pure palm biodiesel in a concentration of 0.32% by weight. The organic substances ethylenediamine (EDA) and terbutylamine (TBA) were added to the blends as corrosion inhibitors in a concentration of 0.1 g/l, as reported in the literature [23]. Subsequently, the efficacy of such inhibitors was evaluated by mass loss tests under total immersion conditions at 45 °C. The presence of corrosion inhibitors in biodiesel was analyzed for carbon steel and copper because those metals showed the

Table 1. Chemical composition of palm biodiesel (% mass).

Type of methyl ester	% mass
Myristic	1.03
Palmitic	43.30
Stearic	4.20
Palmitoleic	0.15
Oleic	41.80
Linoleic	9.10
Linolenic	0.15
Total saturated	48.80
Total unsaturated	51.10

Table 2. Physicochemical properties of palm biodiesel.

Properties	Method	B100
Density at 15 °C (kg/m^3)	ASTM D1298	871.60
Viscosity kinetics at 40 °C (mm^2/s)	ASTM D445	4.67
High calorific value (MJ/kg)	ASTM D240	39.53
Flashpoint (C°)	ASTM D93	162.30
Rancimat Oxidative Stability (h)	EN 14112	12.83
Cloud point (°C)	ASTM D94	18.00
Cetane index	ASTM D976	57.00

3. Results

3.1. Behavior of metals in B100 and blends of B100 and organic acids under different exposure conditions

3.1.1. Behavior of metals in B100 under different exposure conditions and temperatures

The five metallic materials selected in this study were evaluated under different exposure conditions (vapor, partial immersion, and total immersion) in B100 at 25 and 45 °C to determine the effect of such variables on their corrosion processes SS, CS, Sn, and Al did not show significant changes in corrosion rate values when temperature or exposure conditions were varied; therefore, the corrosion rate charts of those metals are not included in this paper.

Stainless steel presented corrosion rates in the order of 3×10^{-5} and 4×10^{-5} mm/year under the three exposure conditions mentioned above after 12 months at 25 and 45 °C, respectively. In turn, aluminum exhibited corrosion rates in the order of 5×10^{-5} mm/year under all three conditions after 12 months of exposure at both temperatures (25 and 45 °C). The corrosion rate of tin was equal to 2×10^{-4} mm/year under all the conditions at 12 months of exposure at both temperatures (25 and 45 °C). Furthermore, CS exposed at 25 and 45 °C displayed a very similar corrosion behavior under all the exposure conditions: higher corrosion rates in the first three months of exposure, which gradually decreased until the end of the test. By contrast, copper exhibited significant changes as well as greater deterioration due to corrosion when such

Table 3. Physicochemical properties of the acid compounds used in the biodiesel blends.

Acid	Molar mass (g.mol^{-1})	Density (g/ml)	Water solubility (mg/l)	Melting point (°C)	Boiling point (°C)	Flash point (°C)
Myristic	228.38	0.99 (24 °C)	20 at (20 °C)	54.40	326.20	110
Palmitic	256.43	0.85 at (25 °C)	7.19 at (20 °C)	62.90	351	206
Stearic	284.48	0.94 at (20 °C)	0.34 at (25 °C)	69.30	361	113
Oleic	282.47	0.89	Insoluble	14	360	189
Acetic	60.05	1.04	Miscible	16	118	40
Linoleic	280.44	0.90	0.13	-5	230	112

greatest corrosion deterioration during the immersion tests in the B100-acid blends.

2.5. Calculation of corrosion rate

To determine the mass loss of the metal due to corrosion, corrosion products were removed from the samples by means of chemical pickling after exposure following the procedures described in ASTM G1. The corrosion rate (CR) was calculated with the mass loss and expressed in mm/yr using the equation (ASTM G1 Section 8.1)

$$CR = (K \times W) / (A \times t \times D) \quad (1)$$

where K is a constant (8.76×10^4); t, exposure time (h); A, area of the exposed metal specimen (cm^2); W, mass loss of the material (g); and D, density of the material (g cm^{-3}).

2.6. Characterization of corrosion products

The corrosion products formed in the metal specimens during immersion in the biodiesel blends were characterized by scanning electron microscopy (SEM) techniques using a JEOL JSM 6490 LV scanning electron microscope, with secondary and backscattered electron detector, along with the analysis of energy-dispersive x-ray spectroscopy (EDS). A Raman spectroscopy analysis was carried out on a Micro-Raman spectrometer, available from Horiba Jovin Yvon, with a wavelength of 784 nm from the light source of an argon laser.

conditions were varied. As a result, this section only analyzes the behavior of copper exposed to pure biodiesel under different conditions and temperatures.

Figure 1 shows the corrosion rate charts of Cu samples evaluated in B100 at 25 and 45 °C after 3, 6, and 12 months under different exposure conditions. Cu exhibited the significant effect of such conditions and temperatures on the corrosion of the metal specimens. Cu in the vapor phase presents very similar corrosion rates at both temperatures. Nevertheless, when partially submerged at 45 °C, the corrosion process of this metal (0.010 mm/year) increases with respect to specimens under the same exposure condition at 25 °C (0.002 mm/year) only during the first 6 months. In the total immersion condition at 45 °C, Cu corrosion rate was higher during the first 6 months of exposure (0.0165 mm/year) and decreased considerably after 12 months (0.0092 mm/year). These results can be compared with data obtained from the literature, which reports that the corrosion deterioration of copper after 20 years is 0.054 mm/year in an industrial atmosphere, 0.050 mm/year in a marine environment, and 0.017 mm/year in a rural context, which corresponds to good resistance to corrosion [24].

The totally immersed Cu at 45 °C showed a 72% higher corrosion rate compared to samples immersed at 25 °C, which shows a significant effect of temperature on Cu corrosion processes when totally immersed in B100. The exposure condition also had an important effect on Cu corrosion, greater deterioration was found in the totally immersed specimens. These results are associated with the fact that Cu acts as a catalyst in the degradation of biodiesel, promoting the oxidation processes of the same and, therefore, oxygen concentration that leads to

corrosive processes in metals. In general, under all conditions, an increase in the copper corrosion rate was observed during the first 6 months of exposure. However, such rate decreased after 12 months of immersion, which indicates that, like CS, Cu can also form a film of corrosion products that restricts the dissolution of the metal, which only happens after long exposure times. The corrosion rate of Cu in B100 at 25 and 45 °C was reduced after 12 months of total immersion by 45 and 42%, respectively.

Comparing such percentages of corrosion rate reduction, it can be said that, as temperature increases, the corrosion rate of copper will be less reduced, thus confirming the inhibitor effect of temperature on the corrosion processes of this metal in biodiesel. The reductions in copper corrosion rates are much lower than those calculated for carbon steel (82% at 25 °C and 83% at 45 °C) in the total immersion condition and long exposure time (12 months) at both temperatures, which leads to the conclusion that the layers formed on the steel surface are more protective than those on copper.

Figure 2 presents the visual appearance of Cu and CS samples exposed to B100 under different temperatures and conditions for one year. As mentioned above, greater deterioration was observed in the samples that were totally immersed in B100. A green patina formed by corrosion products is observed on the surface of the Cu samples that were in direct contact with the biodiesel. CS also shows greater deterioration in the samples immersed in biodiesel, where corrosion is initially formed by pitting and then becomes generalized corrosion.

3.1.2. Behavior of metals in B100-organic acid blends under different exposure conditions

This section evaluates the corrosion behavior of metallic materials under different exposure conditions in biodiesel blends with linoleic, palmitic, and oleic acids at 45 °C.

Figure 3 shows the corrosion rate charts of all the metals considered in this work evaluated at 45 °C under the three exposure conditions (vapor, partial immersion, and total immersion) in a B100-linoleic acid blend. At the end of the test, SS, CS, and Al showed very similar corrosion rate values under the three exposure conditions.

Totally immersed CS presented a decrease of 87.67% in corrosion rate at 12 months of immersion in the blends with linoleic acid. Such value is similar to that calculated for this material in pure B100 (an 83% decrease in corrosion rate), where the products of generalized corrosion on the surface of the immersed samples were remarkable (see Figure 2). These results are associated with the formation of iron oxides on the surface of the metal, which prevent the attack by corrosion along with immersion time. In turn, tin exhibited greater deterioration when exposed in the vapor phase. In general terms, it can be said that, except for Cu, exposure conditions do not affect the corrosion rate of the metals evaluated in this work. In all the cases, after 12 months of exposure, the corrosion rate of metals decreases to values in the range of approximately 1×10^{-4} mm/year. Contrary to the other metals evaluated in the B100-linoleic acid blend, Cu shows a greater deterioration in total immersion, and its corrosion rate increases along with exposure time, reaching values of 0.014 mm/year at 12 months of immersion. This fact can be attributed to the catalytic effect of copper on the oxidation processes of biodiesel. In the B100-palmitic acid blend (corrosion rate charts of metals not included in this paper), the exposure condition had no effect on the corrosion of stainless steel, carbon steel, or tin. The corrosion rate of said metals decreases to values in the order of 1×10^{-6} mm/year after 12 months of exposure. However, aluminum showed the greatest corrosion deterioration in this blend, followed by copper. More specifically, the exposure condition had a significant effect on the corrosion of aluminum and copper, which presented higher corrosion rate values in total immersion; however, like in other metals, such rates decrease after 12 months of exposure. The corrosion rate of aluminum decreased by 16% after 12 months of total immersion in the B100-palmitic blend with respect to its rate during the first 3 months, reaching values of 8×10^{-3} mm/year. Cu corrosion rate decreased by 25% after 12 months of total

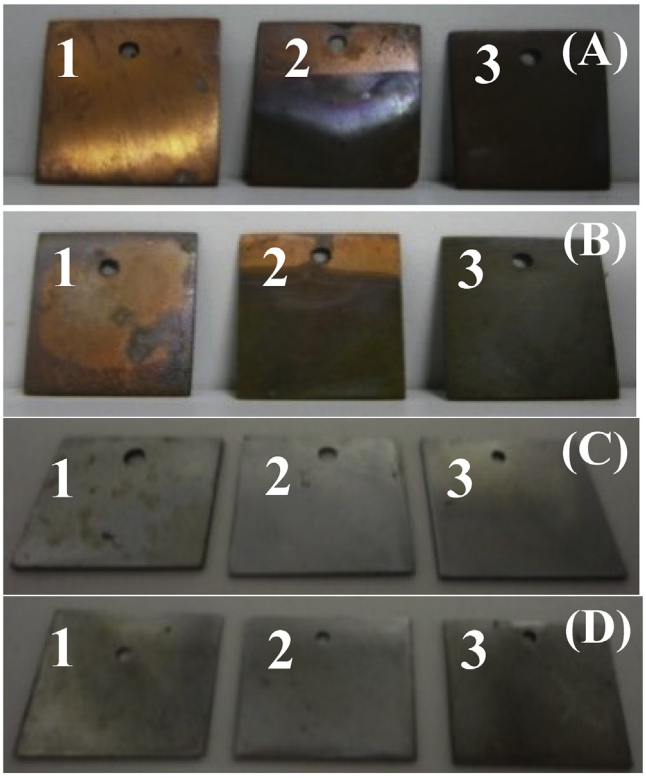

Figure 2. Visual appearance of samples exposed to B100 in (1) vapor phase, (2) submerged, and (3) totally submerged (A) Cu at 25 °C (B) Cu at 45 °C (C) CS at 25 °C, and (D) CS at 45 °C.

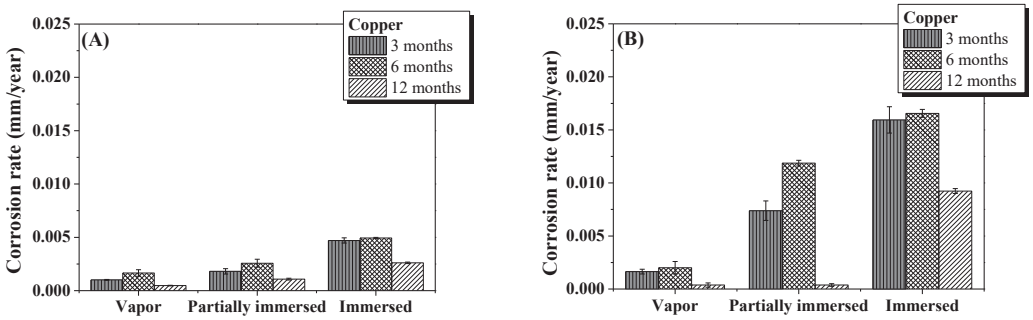

Figure 1. Corrosion rate of copper evaluated in B100 under several exposure periods and conditions. A) 25 °C. B) 45 °C.

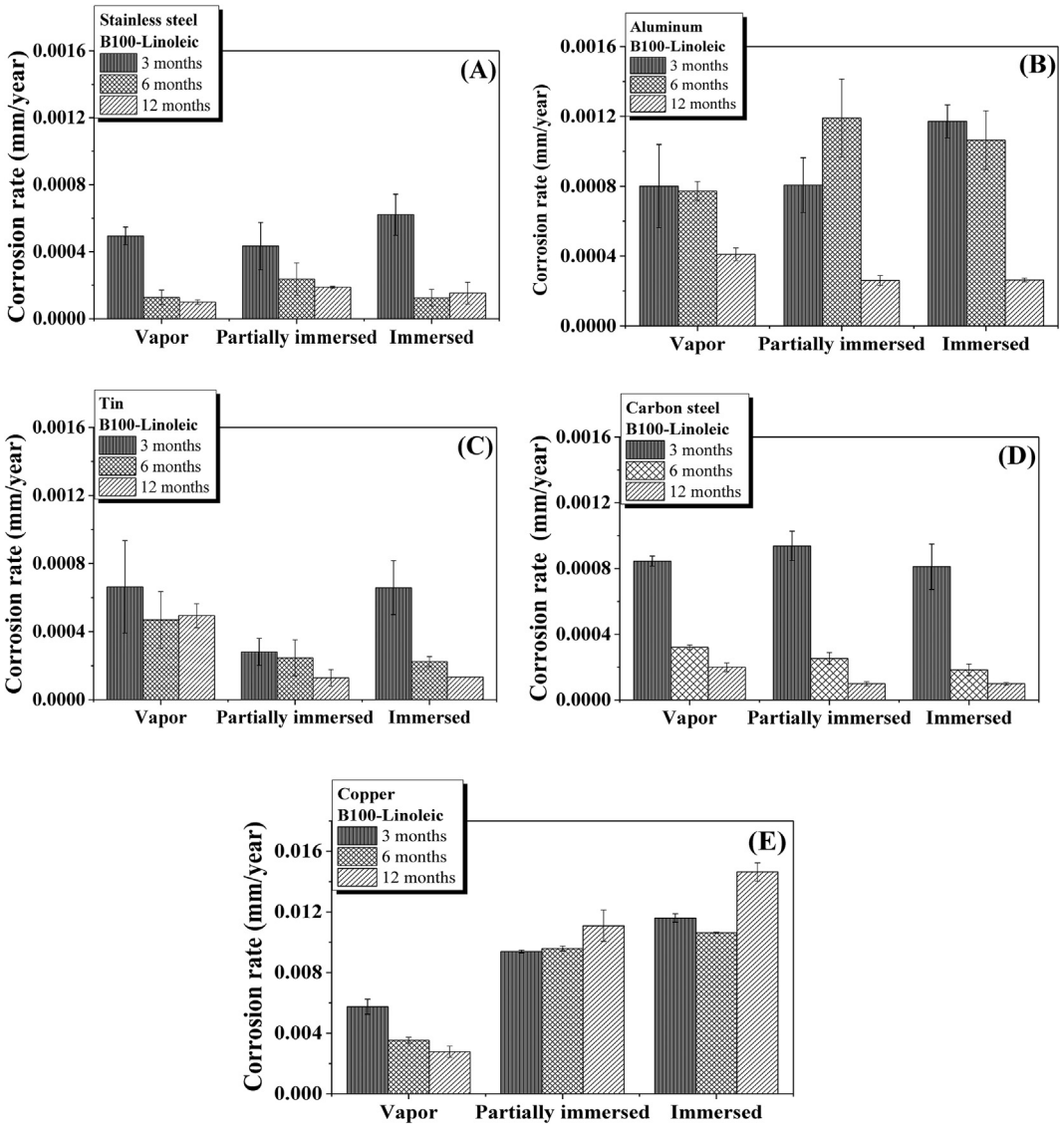

Figure 3. Metals evaluated in the B100-linoleic acid blend under the three exposure conditions at 45 °C(A) Stainless steel (B) Aluminum (C) Tin (D) Carbon steel (E) Copper.

immersion in the B100-palmitic blend, reaching values of 3×10^{-3} mm/year. In the B100-oleic acid blend (corrosion rate charts of metals not included in this paper), the exposure condition had no effect on the corrosion of stainless steel, aluminum, or tin. In that blend, the metals most affected by corrosion were copper and carbon steel, with the highest corrosion rate values in total immersion. CS presented a corrosion rate of 0.043 mm/year at 3 months of immersion, which decreased to 2.4×10^{-4} mm/year after 12 months, i.e., a reduction of 99.4%. The corrosion rate of this metal after 6 months of exposure could not be calculated due to difficulties in the measurements. Copper presented a corrosion rate of 0.0021 mm/year after 3 months of immersion, which then increased to 0.0106 mm/year at 6 months of immersion and finally decreased again to 0.0061 mm/year. This corresponds to a reduction of 43% in the corrosion rate of this metal between 6 and 12 months of immersion. In general, stainless steel showed less corrosion deterioration under all the exposure conditions in all the B100-organic acid blends compared to the other metals evaluated in this study. The opposite was observed for Cu, which was the fastest corroding metal in total immersion in most blends, followed by carbon steel. In all cases, the corrosion rate of carbon steel after 12 months of immersion decreased more than that of copper by the same time. This result is associated with the fact that the protective layers formed on the steel surface when interacting with the B100-acid blends are more stable and protective than those produced on the copper surface when exposed to said blends.

In general, the exposure condition that most affected the metals was total immersion. Therefore, this work analyzes in detail the corrosion behavior of all the metals totally immersed in the blends. According to Aquino [8] samples of copper and brass immersed in commercial biodiesel at 55 °C presented greater mass loss than specimens exposed to the vapor phase, despite being in direct contact with the oxygen of the environment. The increase in the corrosion rate of the metals is attributed to the high concentration of dissolved oxygen; therefore, the increase in oxygen solubility in the biodiesel causes a greater metal loss by corrosion when totally immersed. These results indicate that the oxidation processes, in which thousands of by-products are generated, can increase the percentage of oxygen in biodiesel and make it more corrosive. The dissolved oxygen and contact with metals may increase the corrosive nature of biodiesel due to a rise in the amount of by-products generated by oxidation reactions, such as higher water content and free fatty acids [25].

3.1.3. Comparison of the corrosion behavior of metals under full immersion conditions in different test media at 45 °C

Figures 4, 5, 6, 7, and 8 show the corrosion rate charts of metal samples immersed in test fuels at 45 °C after 3, 6, and 12 months of exposure. The nomenclature in their legends refers to the test media: B100 (pure palm biodiesel), B100-OA (B100-oleic acid blend), B100-LA (B100-linoleic acid blend), B100-MA (B100-myristic acid blend), B100-SA (B100-stearic acid blend), B100-AA (B100-acetic acid blend), and B100-PA (B100-palmitic acid blend).

More specifically, Figure 4 shows the corrosion rate of SS totally immersed in the test fuels after several exposure periods at 45 °C. Such steel, commonly used in exhaust pipes and intake valves, did not exhibit significant mass losses in any of the fuels or after the different immersion times. However, the specimens exposed to 6 months of immersion in B100 displayed corrosion rates of 0.0001 mm/year, which then decreased to 0.00003 mm/year after 12 months. The highest corrosion rate values of this metal were observed in the B100-LA and B100-SA blends, where its samples reached 0.0006 mm/year after 3 months of immersion that then decreased to 0.0001 mm/year and 0.00005 mm/year, respectively. Such behavior was observed in all the blends, suggesting a passivation of the stainless steel. These results can be used to establish an ascending order of the aggressiveness of the acids on the corrosion of stainless steel, taking pure biodiesel as the reference point: B100 ˂ B100-OA ˂ B100-MA ˂ B100-AA ˂ B100-PA ˂ B100- LA ˂ B100-SA.

Figure 5 shows the corrosion rates of tin after several periods of exposure totally immersed in the test fuels at 45 °C. The addition of organic acids to the biodiesel had no effect on the corrosion of tin because said material exhibited a greater corrosion attack in B100 at 3 months of immersion (0.0027 mm/year); then, the material was passivated until the end of the test (0.00009 mm/year).

Figure 6 details the corrosion rates of Al after several exposure periods totally immersed in the test fuels at 45 °C. The corrosion rates of aluminum, as well as stainless steel, decreased significantly after 12 months of exposure. Very low corrosion rates are observed in B100 compared to the values obtained in the other immersion media. Al presents the highest corrosion rate values in the blend of B100 with palmitic acid at 3 months of total immersion (0.0106 mm/year). However, the corrosion rate of aluminum in all media decreases at 12 months of exposure. Hence, the effect of the acids on aluminum corrosion can be formulated in an ascending order, as follows: B100 ˂ B100-OA ˂ B100-SA ˂ B100-LA ˂ B100-MA ˂ B100-AA ˂ B100-PA.

In turn, Figure 7 is the corrosion rate chart of CS after several periods of exposure totally immersed in the test fuels at 45 °C. The CS exposed in the blend with oleic acid showed the highest corrosion rates among all the metals (0.0433 mm/year). In this material, a morphology of localized corrosion (few scattered points) was initially observed; it then became generalized corrosion with detachment of corrosion products and significantly higher mass losses compared to those of the same material in B100. These results demonstrate that oleic acid significantly affects carbon steel; however, its corrosion rate decreases along with immersion time to 0.0002 mm/year after 12 months in the blend. A similar behavior was observed in CS in the B100 blends with the other acids: corrosion rate values decrease considerably after 12 months of exposure. The effect of the acids on the corrosion of carbon steel can be expressed in an ascending order, as follows: B100-SA ˂ B100-AA ˂ B100-OA ˂ B100-LA ˂ B100 ˂ B100-MA ˂ B100-OA.

Figure 8 illustrates the corrosion rate of copper after several exposure periods totally immersed in the test fuels at 45 °C. In the blends with palmitic, oleic, myristic, and stearic acids, copper formed a protective oxide layer, presenting higher corrosion rates in the first 3 months, which then decreased until the end of the test. Unlike the other metals evaluated in this work, Cu immersed in the blends with linoleic and acetic acids underwent greater corrosion deterioration over the immersion time. In the blend of B100 with linoleic acid, copper exhibited values of 0.0116 mm/year after 3 months of total immersion and 0.0143 mm/year after 12 months. The high corrosivity of the biodiesel blend with linoleic acid is due to the fact that this acid is unsaturated, i.e., it has two double bonds. Therefore, the hydrogens of the allylic and double ally positions are readily oxidizable. This leads to the oxidation of biodiesel, which produces an increase in its corrosivity. The acid that affected copper the most was acetic acid; it generated a corrosion rate of 0.0135 mm/year after 3 months of immersion, which then increased to 0.0229 mm/year after 12 months. The effect of the acids on copper corrosion can be classified as follows: B100-SA ˂ B100-MA ˂ B100-PA ˂ B100-OA ˂ B100 ˂ B100-LA ˂ B100-AA.

In general, CS and Cu were the most affected materials by the immersion in B100 and B100-acid blends.

3.2. Characterization of corrosion products of copper and carbon steel exposed to B100 and B100-blends of organic acids

The characterization of corrosion products was performed only for Cu and CS, as said metals suffered more deterioration by corrosion than the other materials evaluated in this work. The low corrosion rates found in Al, Sn, and SS under the different evaluation conditions limited the possibility of extracting corrosion products for characterization. Figure 9 presents the surface morphology of CS after 12 months of exposure to B100 at 45 °C, where iron oxides can be observed because of the localized corrosion.

Figure 9A shows some of the holes caused by the eruption of bubbles formed on the steel surface; they look similar to “craters”, which means that the generation of corrosion products mainly began at the sites where

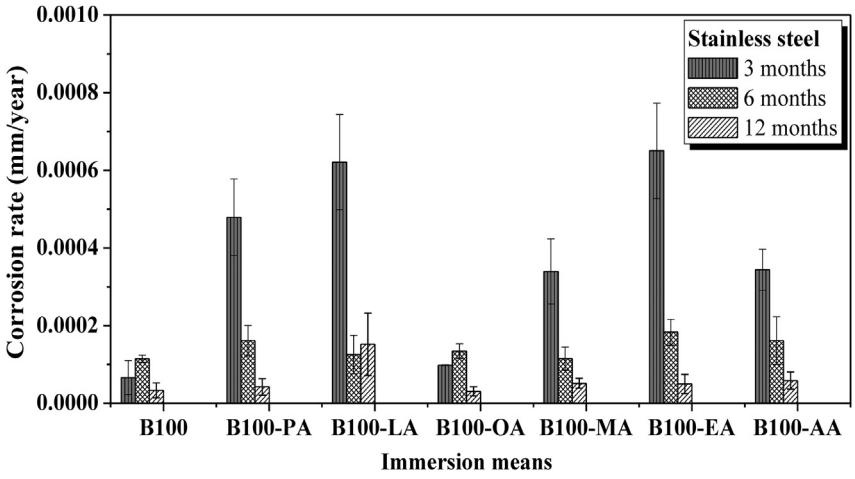

Figure 4. Corrosion rate of stainless steel after several periods of exposure totally immersed in the test fuels at 45 °C.

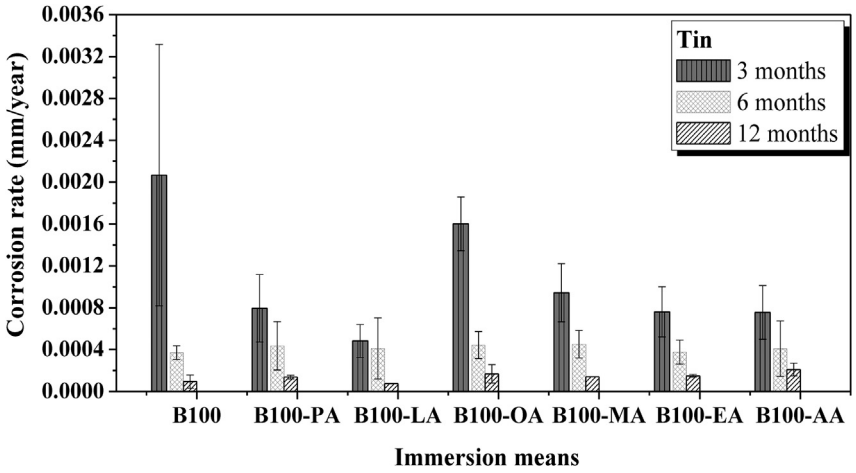

Figure 5. Corrosion rate of tin after several periods of exposure totally immersed in the test fuels at 45 °C.

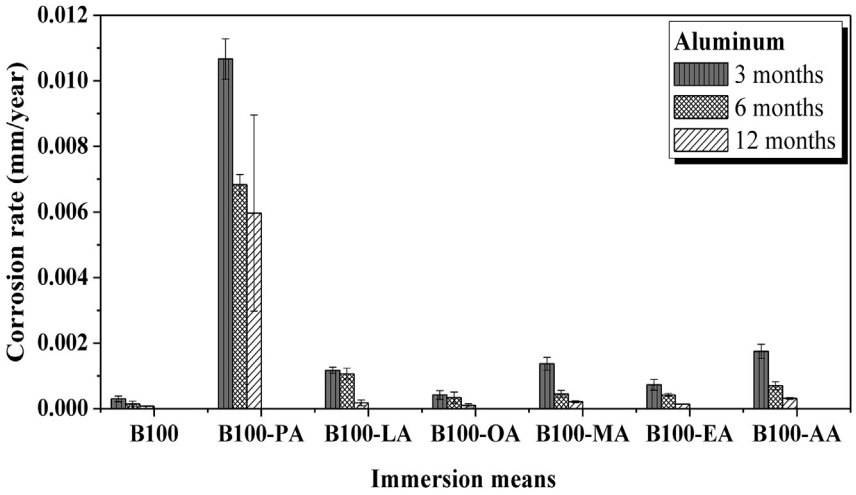

Figure 6. Corrosion rate of aluminum after several periods of exposure totally immersed in the test fuels at 45 °C.

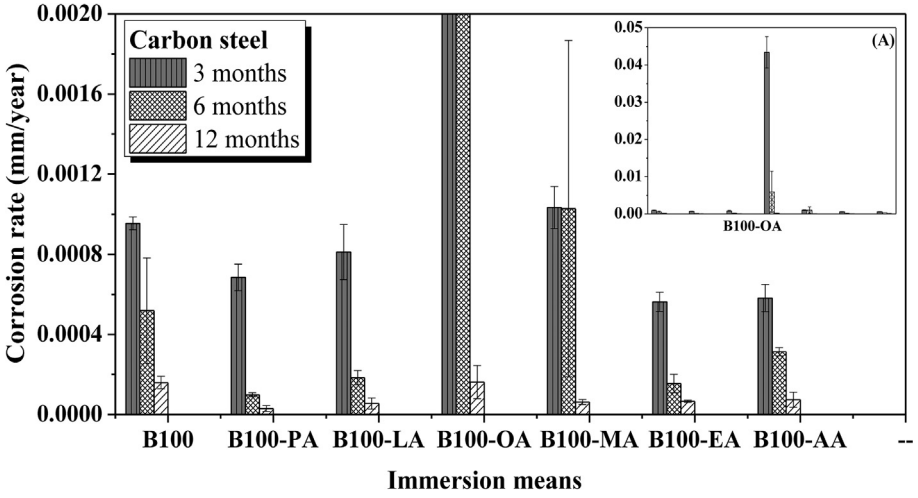

Figure 7. Corrosion rate of carbon steel after several periods of exposure totally immersed in the test fuels at 45 °C(A) B100-OA.

localized corrosion was present. Such bubbles are formed on the surface of the metal because of the accumulated pressure they contain. They grow due to the pressure of the gases inside them until they burst, which allows the entry of oxygen and, therefore, the formation of oxides [26].

In this work the corrosion products on the steel surface were analyzed by EDS to investigate the composition and quantity of the elements that were found (see Figure 9B). Such analysis indicates that the main elements present in the corrosion products of steel are O, C, and Fe, which

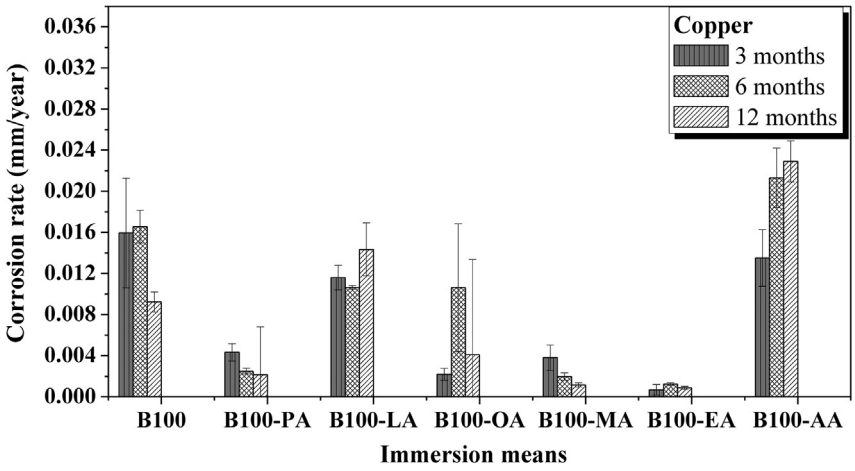

Figure 8. Corrosion rate of copper after several periods of exposure totally immersed in the test fuels at 45 °C.

proves the presence of iron oxides, hydroxides, oxyhydroxides, iron carbonates, and salts of fatty acids on the metal surface [14]. The high percentage of oxygen in the corrosion products of steel in B100 at 45 °C (36.97%) indicates a high concentration of different oxides inside the wells formed by the corrosion attack. The oxygen that favors the formation of said oxides is dissolved in biodiesel because the fuel absorbs water and CO_2 from the environment as a consequence of its hygroscopic character [3]. The presence of water in the biodiesel under evaluation, is also due to the hydrolysis and oxidation reactions of biodiesel during the test time. In addition, oxygen concentration can be increased by extending immersion time due to the generation of different types of fatty and organic acids from the reactions of oxidation of biodiesel, which can accelerate the rate of corrosion [27]. The presence of carbon (13.95%) in the corrosion products of the steel is due to the absorption of CO_2 from the environment and to the $RCOO^-$ radicals from esters and carboxylic acids generated from the oxidation reactions of biodiesel [3]. The carbon also can be present in corrosion products due to formation of organic deposits as a consequence of the decomposition of fatty acids and other acids that react with metallic oxides [8].

Figure 10 is the Raman spectrum plot of CS samples after 12 months' exposure in B100 at 45 °C. Typical Raman bands reported in the literature for compounds commonly found in the corrosion products of carbon steel can be observed in the Figure. The Raman spectrum of steel shows bands that correspond to the presence of one or more species associated with lepidocrocite (L: γ-FeO (OH)), ferrihydrite $5Fe_2O_3 \bullet 9H_2O$), magnetite (M: Fe_3O_4), hematite (H: α-Fe_2O_3), and siderite (S: $FeCO_3$). The formation of these oxides and hydroxides is attributed to the reactions between iron and water or oxygen. The formation of $FeCO_3$ can be attributed to the reactions between iron and $RCOO^-$ radicals. Several aspects can be identified in the spectrum of steel immersed in B100 for 12 months: an intense peak at 662 cm^{-1} (associated with a mixture of magnetite [28] and ferrihydrite [29] and moderate bands located at 345 cm^{-1} (attributed to the formation of lepidocrocite) and 405 cm^{-1} (related to a mixture of hematite and ferrihydrite [30]). Weak bands were also observed at 1082 cm^{-1} (associated with siderite formation [30]) and at 1310 cm^{-1} (attributed to hematite formation [28]). The corrosion rate of carbon steel immersed in B100 decreased by 84% at 12 months of immersion, which confirms the protective effect of the layer formed on the surface of the metal composed of the mixture of oxides such as magnetite and siderite. Magnetite has a very small crystal size and tends to compact much in the inner layers of the rust, where there is no oxygen access.

The reactions that explain the formation of the corrosion products of carbon steel in contact with biodiesel for 12 months at 45 °C (See Figure 10) can be described as follows:

Metallic iron combined with oxygen to form hematite that, in turn, reacts with water to form ferrihydrite.

$$4Fe + 3O_2 \rightarrow 2Fe_2O_3 \quad (4)$$

$$Fe(OH)_3 \rightarrow Fe_2O_3 + H_2O \quad (5)$$

$$5\alpha - Fe_2O_3 + 9H_2O \rightarrow 5Fe_2O_3.9H_2O \quad (6)$$

The RCOO and –COOH radicals generated from the methyl esters and fatty acids present in biodiesel can react with iron ions and iron oxides to form iron carbonates (siderite) [3]:

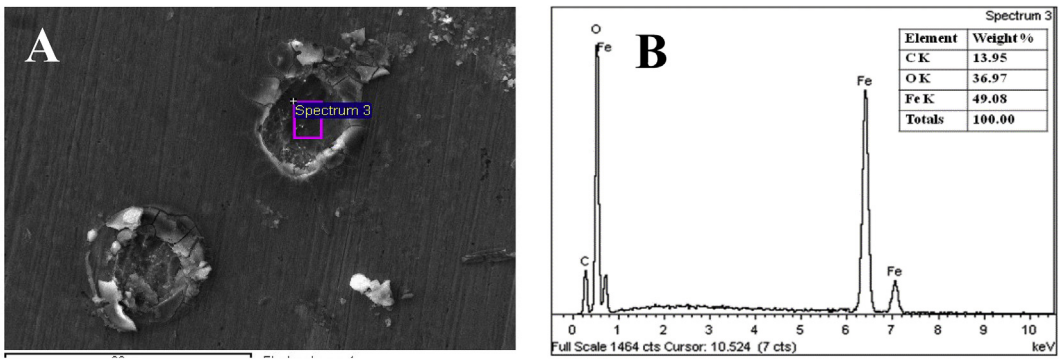

Figure 9. SEM images and EDS analysis of the surface of carbon steel immersed in B100 for 12 months at 45 °C (A) Craters produced on the steel surface surrounded by corrosion products (B) EDS of the wells formed on the steel surface.

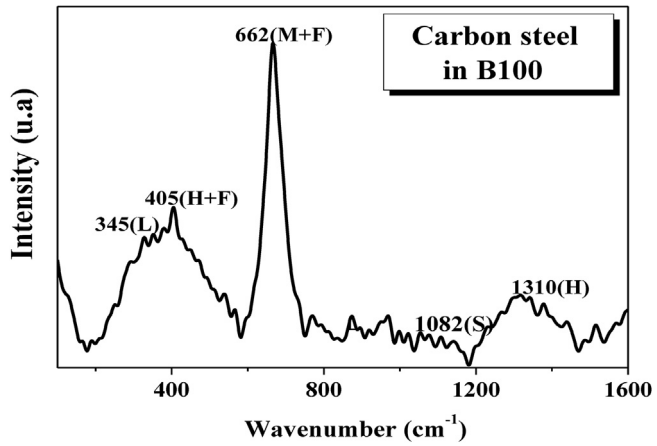

Figure 10. Raman spectra of carbon steel exposed to B100 for 12 months at 45 °C.

$$Fe^{2+} + 2RCOO^{\cdot} \rightarrow FeCO_3 + R - R + CO_2 \quad (7)$$

Iron oxide II reacts with iron oxide III to form the magnetite:

$$FeO + Fe_2O_3 \rightarrow Fe_3O_4 \quad (10)$$

Iron hydroxide II reacts with oxygen to form iron hydroxide III [31] and lepidocrocite (γ-FeOOH) [32]:

$$4Fe(OH)_2 + O_2 + H_2O \rightarrow 4Fe(OH)_3 \quad (11)$$

$$4Fe(OH)_2 + O_2 \rightarrow 4\gamma - FeOOH + 2H_2O \quad (12)$$

$$2FeO + 2H_2O \rightarrow FeOOH + H_2 \quad (13)$$

Figure 11 depicts the morphology of the copper surface exposed to B100. An analysis of the corrosion products on the copper surface in B100 by EDS indicated a high concentration of carbon (52.6 %) and oxygen (28.5%), which is attributed to the formation of oxides, hydroxides, copper carbonates, and salts of fatty acids (see Figure 12).

The formation reactions of the possible corrosion products generated on the surface of copper in contact with biodiesel for 12 months at 45 °C can be described as follows:

Formation of copper oxides due to the presence of dissolved oxygen and water:

$$2Cu + O_2 \rightarrow 2CuO \quad (16)$$

$$4Cu + O_2 \rightarrow 2Cu_2O \quad (17)$$

Formation of copper carbonates from the reaction between ions, oxides, and copper hydroxides and CO_2, O_2, $RCOO^-$, and COO^- [3]:

$$Cu(OH)_2 + COO^- \rightarrow Cu(OH)_2.CuCO_3 \quad (20)$$

$$2Cu(OH)_2 + CO_2 \rightarrow Cu(OH)_2.CuCO_3 + H_2O \quad (21)$$

$$2Cu + H_2O + CO_2 + O_2 \rightarrow Cu(OH)_2.CuCO_3 \quad (22)$$

These corrosion products tend to settle in areas where mechanical movement of certain components occurs, such as bearings in fuel pumps and fuel injectors. This would result in accelerated wear on the component surfaces.

3.3. Evaluation of the corrosion of copper and carbon steel in B100 and blends of B100-organic acids with corrosion inhibitors

The corrosion rate of metals exposed to B100 and blends of B100-organic acids may decrease over time if an organic monomolecular film is formed at the metal-liquid interface by cationic/anionic corrosion inhibitors used in the fuel industry, which avoids the direct contact of the metal with biodiesel [33]. Compounds based on amines including primary amines, diamines, amine-amines, and oxyalkylated amines are effective corrosion inhibitors in fuels [34]. The mechanism of action of amines is to form an organic monolayer adsorbed between the metal-solution interface at potentially catalytic metal surface reactive sites, which avoids direct contact of the active metal with the liquid fuel and prevents the attack of oxygen and moisture [5]. In general, these organic compounds are adsorption-type inhibitors (a common type of inhibitors that form a protective layer) by physical or chemical absorption on the metal surface. Such compounds form a stable bond with the

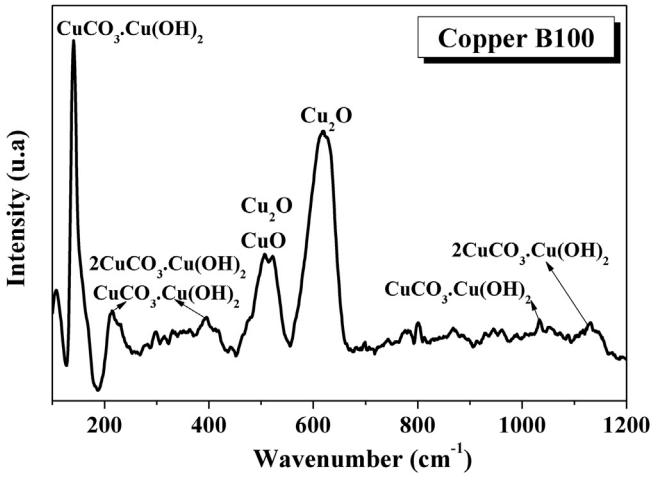

Figure 12. Raman spectra of copper exposed to B100 for 12 months at 45 °C.

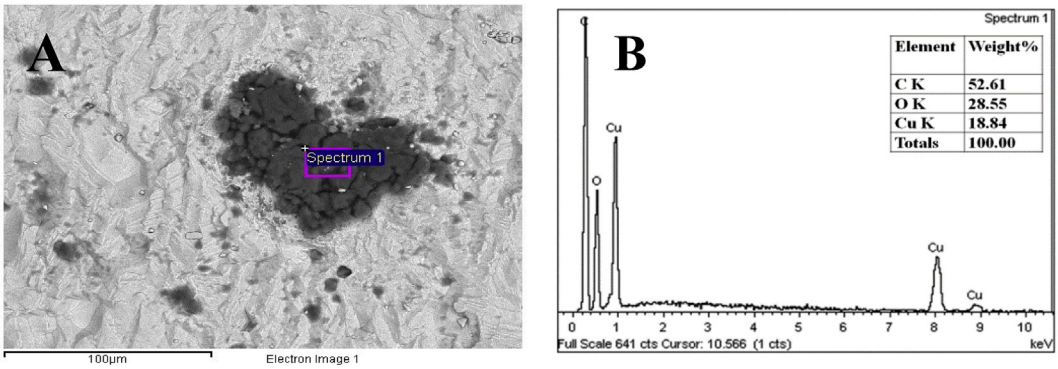

Figure 11. Corrosion products formed on the surface of copper immersed for 12 months in B100 at 25 °C (A) SEM images (B) EDS analysis.

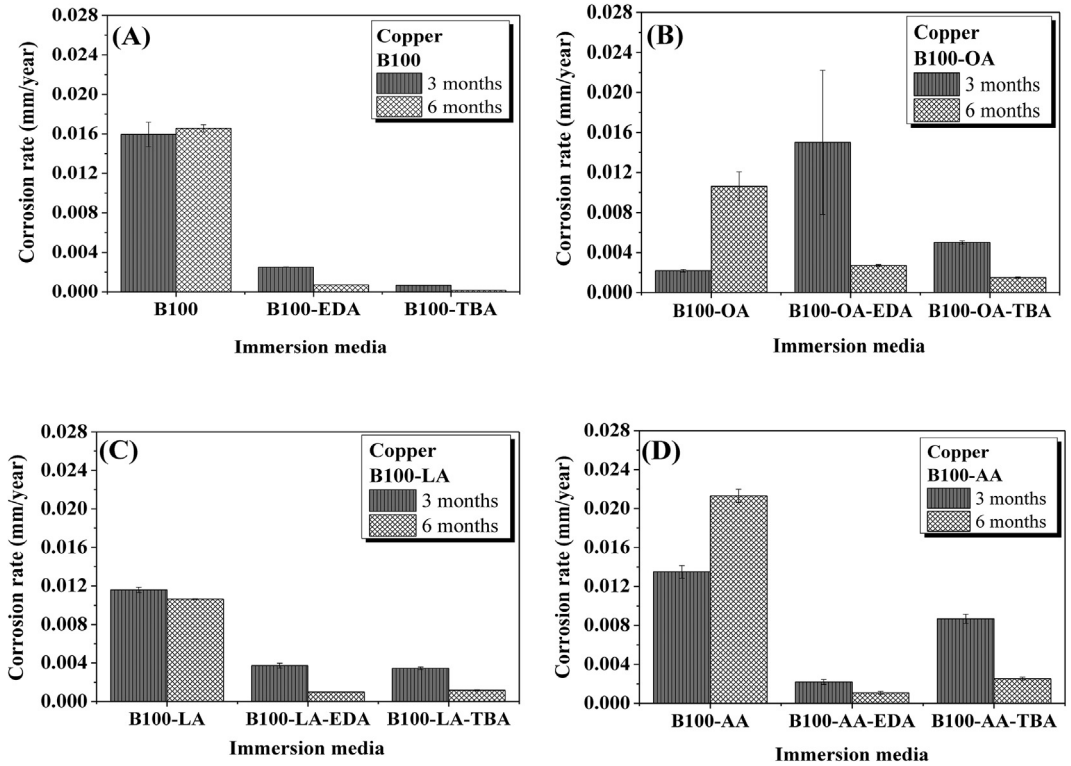

Figure 13. Corrosion rate of copper totally immersed in B100-acid-corrosion inhibitor blends after various exposure periods at 45 °C(A) B100 (B) B100-OA (C) B100-LA (D) B100-AA.

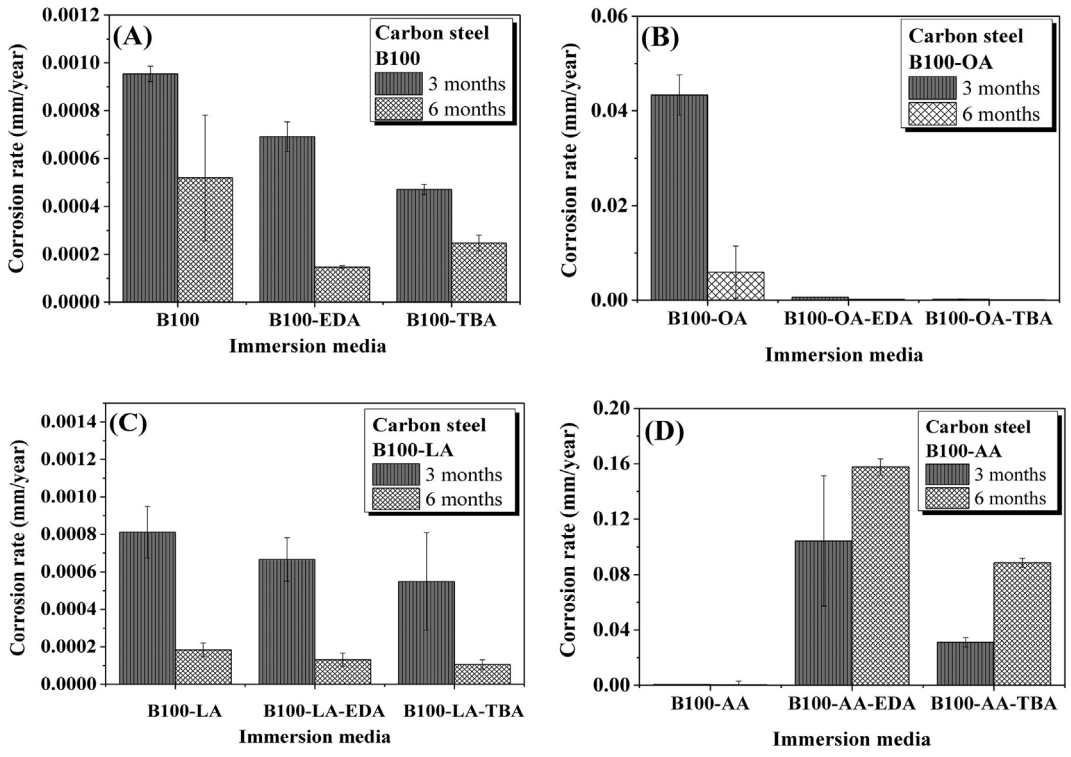

Figure 14. Corrosion rate of carbon steel totally immersed in B100-acid-corrosion inhibitor blends at 45 °C at various periods of exposure (A) B100 (B) B100-OA (C) B100-LA (D) B100-AA.

surface of the metal when they are adsorbed into it [23]. The corrosion rate decreases as the surface adsorption is completed.

The effect of the corrosion inhibitors ethylenediamine (EDA) and terbutylamine (TBA) was evaluated on Cu and CS because said the metallic materials showed the greatest corrosion damage in B100 and

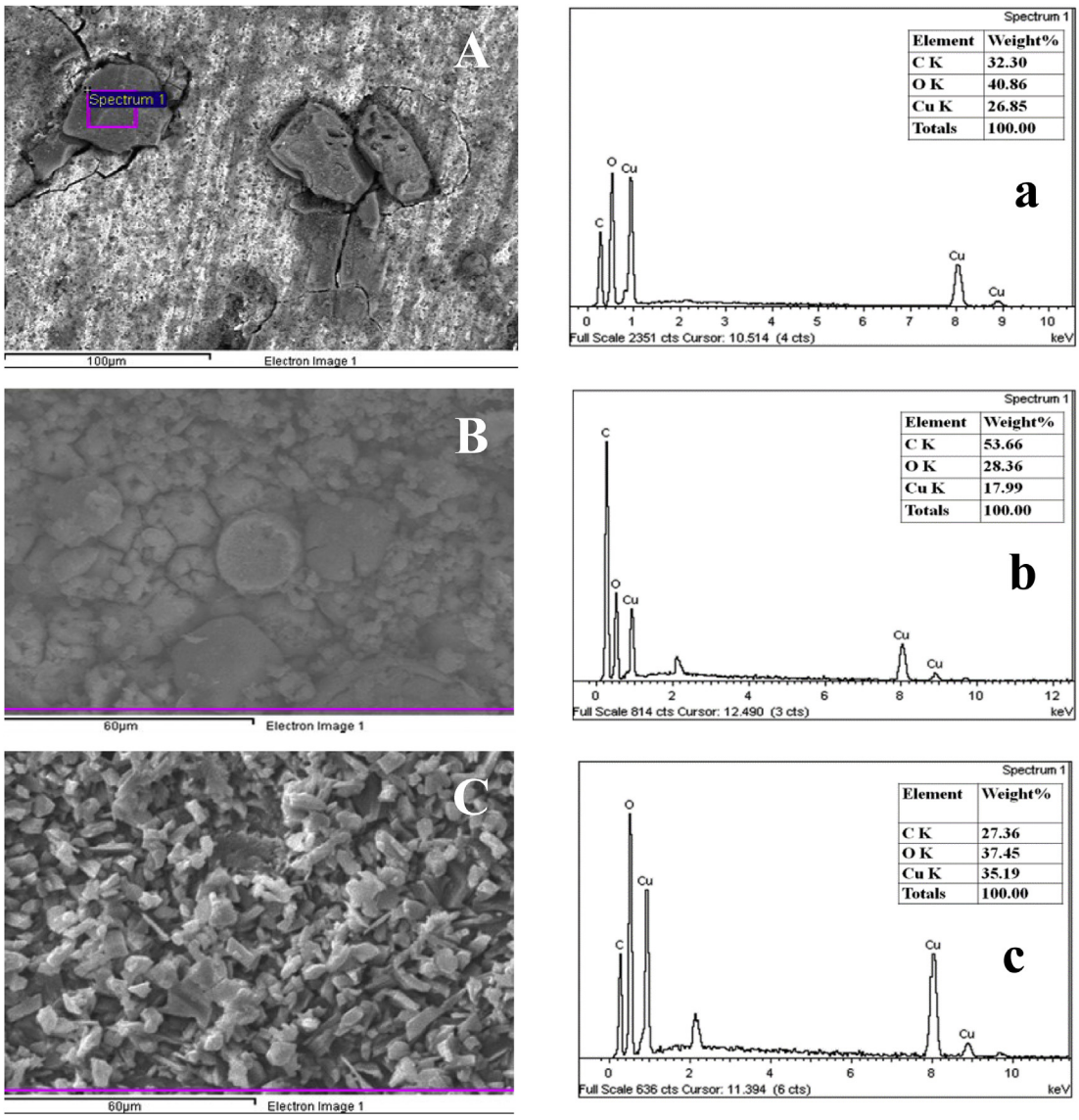

Figure 15. (A) Surface morphology of copper immersed in B100-acetic acid at 45 °C, with generalized corrosion. (a) EDS of corrosion products formed on the copper surface (B) morphology of the protective layer formed on the surface of copper immersed in B100-acetic acid-EDA. (b) EDS of the protective layer formed on copper by the addition of EDA (C) Morphology of the protective layer formed on the copper surface immersed in B100-acetic acid-TBA. (c) EDS of the protective layer formed in the copper by the addition of TBA.

B100-organic acid blends. The corrosion inhibition efficiency of the amines EDA and TBA was calculated by the following equation [35]:

$$\textit{Inhibition efficiency } (IE\%) = \frac{V_{corr} - V_{corr-inh}}{V_{corr}} x100 \quad (23)$$

where $_{Vcorr\text{-}inh}$ and V_{corr} are the corrosion rate values of the metals in the test fuels with and without inhibitor, respectively. The efficiency of the inhibitors was calculated based on the comparison of the corrosion rate values of the metals after 6 months of immersion.

Figure 13 presents the corrosion rate charts of Cu evaluated in fuel blends with organic acids and corrosion inhibitors. The corrosion rate of Cu in B100-EDA decreased by 95.7% and, in B100-TBA, by 98.9% over 6 months of exposure, which shows that TBA is more efficient than EDA at inhibiting Cu corrosion processes in B100.

In the B100-oleic acid blend, Cu exhibits a corrosion rate of 0.0021 mm/year after 3 months, which increases in the same blend with ethylenediamine to 0.015 mm/year and, with tert-butylamine, to 0.005 mm/year. However, after 6 months, the corrosion rate of copper in the B100-oleic acid-ethylenediamine blend decreases by 74.5% and, in B100-oleic-terbutylamine, by 85.8%. In turn, the corrosion rate of Cu in the B100-oleic acid-EDA blend at 6 months of immersion is very similar to that of said metal in the B100-oleic acid blend without the inhibitor. This result indicates that the efficiency of the EDA in this blend is not sufficient to inhibit Cu corrosion. The efficiency of TBA in the B100-oleic acid blend is satisfactory after 6 months of exposure; however, during the first 3 months, this shows that both TBA and EDA accelerate copper corrosion processes.

This fact can be associated with the formation of films on the Cu surface from the corrosion products generated by this material during the first 3 months. The inhibitors of Cu corrosion processes in the B100-linoleic acid blend reached efficiencies of 90.6% (EDA) and 89% (TBA). In the B100-acetic acid blend, Cu presents higher corrosion rate values after 6 months of exposure than after 3 months. In said blend, Cu does not form protective layers during the time of the test. These corrosion rates are greatly reduced by the effect of the inhibitors until the end of the test. The corrosion inhibition efficiency of Cu in the B100-acetic acid-EDA blend was 94.9% and, with the addition of TBA, 88.1%. In general, the efficiency of the corrosion inhibitors EDA and TBA

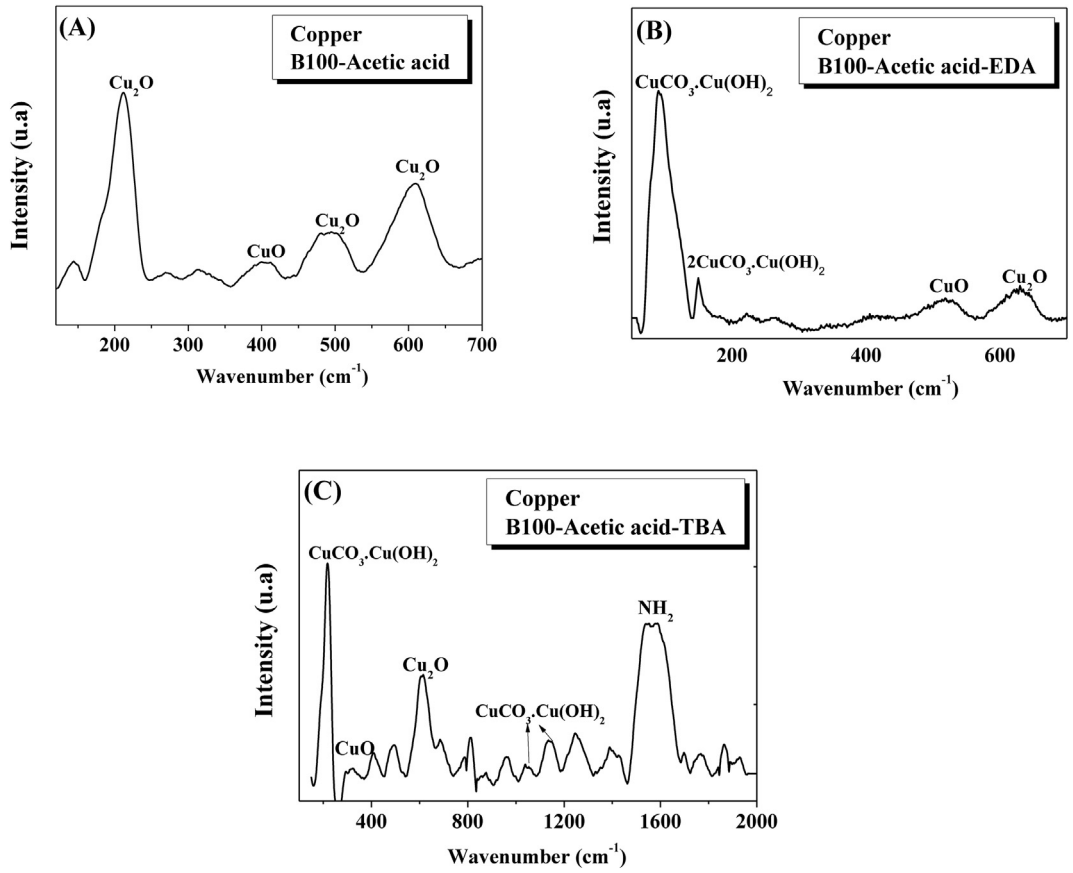

Figure 16. Raman spectra of copper totally immersed in the test fuels at 45 °C for 6 months (A) B100-AA (B) B100-AA-EDA, and (C) B100-AA-TBA.

increases after 6 months of immersion in all media, with decreasing corrosion rate values until the end of the test. However, in the case of Cu, the inhibition efficiency of the amines is lower in the blends with acids than in B100. This fact can be attributed to a greater oxidation of the blends by the presence of acids in comparison to pure biodiesel and, therefore, a greater reactivity between the amines and the acids because amines are bases that, when reacting with acids and esters, can form amine salts [23].

Figure 14 shows the corrosion rate charts of CS in different fuel blends with organic acids and corrosion inhibitors. In B100, EDA and TBA exhibited steel corrosion inhibition efficiencies of 71.8% and 52.4%, respectively. In the B100-oleic acid blend, CS presents a corrosion rate of 0.0433 mm/year after 3 months of immersion, which decreases to 0.0089 mm/year after 6 months. With the addition of EDA and TBA to the B100-oleic acid blend, such corrosion rate values decrease considerably, achieving corrosion inhibition efficiencies of 96.9% and 98.3%, respectively.

In the case of steel in the B100-linoleic acid blends, EDA showed a corrosion inhibition efficiency of 28% and TBA, 45%. In B100-acetic acid-EDA and B100-acetic acid-TBA, carbon steel exhibits much higher corrosion rate values than in the B100-acetic acid blend without the added inhibitors; this suggests that the acetic acid reacts with EDA and with TBA to increase the corrosion processes in this material. The amines EDA and TBA are bases that, when reacting with acidic compounds present in biodiesel (in our case, with acetic acid), can generate neutralization reactions that produce salts and water, which leads to an increase in the corrosively of the medium [23]. The salts produced by this type of reaction seem to have a greater effect on the corrosion deterioration of steel than that of copper. In general, regarding CS, TBA showed higher efficacy in blends with long chain organic acids (oleic and linoleic acids). In general terms, the inhibitors they evaluated achieved less inhibition in steel than in copper.

Figure 15A shows the morphology of the corrosion products formed on the surface of Cu immersed in the B100-acetic acid blend, where it presented greater corrosion deterioration. In turn, Figure 15 B presents the morphology of the layer formed on the Cu surface when exposed to B100-acetic-EDA and B100-acetic-TBA, respectively.

The corrosion products of Cu exposed to the B100-acetic acid blend and those of the layer formed in this material upon contact with the corrosion inhibitors EDA and TBA, individually added to B100-acetic acid, were analyzed by EDS in order to investigate the composition and quantity of the elements present in the sample.

Such analysis indicated the presence of oxygen and carbon. The presence of oxygen is associated with the water content of acetic acid ($C_2H_4O_2$) and other possible chemical species (such as alcohols and fatty acids) formed in biodiesel because of oxidation processes. The amount of carbon was found to be higher on the surface of Cu specimens exposed to the corrosion inhibitors EDA ($C_2H_8N_2$) and TBA ($C_4H_{11}N$), which corroborates the presence of a protective layer formed by the effect of the amines.

Figure 16 is the Raman spectra of the Cu samples exposed to B100-AA, B100-AA-EDA, and B100-AA-TBA. In the spectrum of copper in B100-AA, bands are observed at 213 cm^{-1}, 495 cm^{-1}, and 608 cm^{-1}; all of them are associated with cuprite (Cu_2O) [36]. The band at 405 cm^{-1} is attributed to the presence of tenorite (CuO) [37]. It appears that cuprite and tenorite are not protective oxides when copper is exposed to the B100-AA blend, since its corrosion rate increased by 41% after 12 months of total immersion in the blend.

When Cu was exposed to B100-AA-EDA, cuprite and tenorite oxides were formed, in addition to Cu carbonates such as malachite at 100 cm^{-1} [38] and azurite at 150 cm^{-1}, which have a protective effect on copper, reducing its corrosion rate by 94.9%. With the addition of TBA, we observed the presence of cuprite at 600 cm^{-1}, azurite at 839 cm^{-1}, and malachite at 219 cm^{-1} [39]. A strong band at 1600 cm^{-1} is attributed to

the stretching of the amine group (NH_2) of the TBA, a result that is associated with the presence of a protective monolayer on the surface of the metal, since its corrosion rate was reduced by 81% at 6 months of immersion. The corrosion rate of Cu in B100 decreases by 42% after 12 months of immersion, which is associated with the protective effect of the copper carbonates formed on its surface when interacting with the RCOO- radicals and the reactions between CuO and the CO_2 absorbed by biodiesel. When the spectra of the Cu exposed to B100 and to the blends B100-AA-EDA and B100-AA-TBA are compared, it can be observed that, in all the blends, azurite and malachite copper carbonates were formed in addition to cuprite and tenorite oxides. In B100, B100-AA-EDA, and B100-AA-TBA, a significant reduction of Cu corrosion rates was observed. In B100-AA, copper presented an increase in its corrosion rate until the 12th month of immersion; and the presence of cuprite and tenorite was observed only at the end of the exposure, a result attributed to the low stability of such oxides in said blend. Therefore, the formation of azurite and malachite carbonates is associated with a defensive layer that protects copper over time, a protection that increases with the presence of EDA and TBA as a monolayer adsorbed on the surface of the metal.

4. Conclusions

The highest values of corrosion rates were found in Cu (B100-acetic acid blend) and CS (B100-oleic acid blend) totally immersed. The most corrosive blends for the materials were: B100-linoleic acid, B100-oleic acid, and B100 acetic acid. CS and Cu were the most affected by the immersion in blends. TBA was more effective in inhibiting copper corrosion in B100; in turn, EDA was more effective in the blends B100-oleic acid, B100-linoleic, and B100-acetic acid. In the case of carbon steel in B100, EDA was more effective; and, in B100-linoleic acid and B100-oleic acid, TBA was more effective. Neither inhibitor was effective in the B100-acetic acid blend. Lepidocrocite, magnetite, ferrihydrite, and siderite were the corrosion products found on the surface of CS immersed in the fuels. Such products formed a protective layer that grows and becomes more compact along with immersion time. Tenorite, cuprite, malachite, and azurite were found in Cu immersed in the fuels.

Declarations

Author contribution statement

Libia Baena: Performed the experiments; Analyzed and interpreted the data; Wrote the paper.

Jorge Calderon: Conceived and designed the experiments; Analyzed and interpreted the data; Contributed reagents, materials, analysis tools or data.

Funding statement

This research did not receive any specific grant from funding agencies in the public, commercial, or not-for-profit sectors.

Competing interest statement

The authors declare no conflict of interest.

Additional information

No additional information is available for this paper.

References

[1] M. Fazal, A. Haseeb, H. M.- Energy, and undefined, Degradation of Automotive Materials in Palm Biodiesel, Elsevier, 2012. Accessed: Feb. 15, 2018. [Online]. Available: https://www.sciencedirect.com/science/article/pii/S0360544212001211.

[2] A. de Carvalho, E. Cardoso, G. da R.- Fuel, and undefined, Carboxylic Acid Emissions from Soybean Biodiesel Oxidation in the EN14112 (Rancimat) Stability Test, Elsevier, 2016. Accessed: Feb. 15, 2018. [Online]. Available: https://www.sciencedirect.com/science/article/pii/S0016236115013332.

[3] M. Fazal, A. Haseeb, H. Masjuki, Corrosion mechanism of copper in palm biodiesel, Corros. Sci. (2013). Accessed: Sep. 01, 2017. [Online]. Available: http://www.sciencedirect.com/science/article/pii/S0010938X12004891.

[4] Biodiesel compatibility with carbon steel and HDPE parts, Fuel Process. Technol. 90 (9) (Sep. 2009) 1175–1182.

[5] A. Kovécs, J. Tóth, G. Isaák, I. K.-F. P. Technology, and undefined, Aspects of Storage and Corrosion Characteristics of Biodiesel, Elsevier, 2015. Accessed: Feb. 15, 2018. [Online]. Available: https://www.sciencedirect.com/science/article/pii/S0378382015000296.

[6] D. Jin, X. Zhou, P. Wu, L. Jiang, H. G.-R. Energy, and undefined, Corrosion Behavior of ASTM 1045 Mild Steel in Palm Biodiesel, Elsevier, 2015. Accessed: Feb. 16, 2018. [Online]. Available: https://www.sciencedirect.com/science/article/pii/S0960148115002049.

[7] K. Sorate, P. B.-R. and S. E. Reviews, and undefined, Biodiesel Properties and Automotive System Compatibility Issues, Elsevier, 2015. Accessed: Feb. 15, 2018. [Online]. Available: https://www.sciencedirect.com/science/article/pii/S1364032114007655.

[8] I.P. Aquino, R.P.B. Hernandez, D.L. Chicoma, H.P.F. Pinto, I.V. Aoki, Influence of light, temperature and metallic ions on biodiesel degradation and corrosiveness to copper and brass, Fuel 102 (Dec. 2012) 795–807.

[9] S. Flitsch, P.M. Neu, S. Schober, N. Kienzl, J. Ullmann, M. Mittelbach, Quantitation of aging products formed in biodiesel during the rancimat accelerated oxidation test, Energy Fuels 28 (9) (Sep. 2014) 5849–5856.

[10] S. Norouzi, F. Eslami, M.L. Wyszynski, A. Tsolakis, Corrosion effects of RME in blends with ULSD on aluminium and copper, Fuel Process. Technol. 104 (Dec. 2012) 204–210.

[11] D.-L. Cursaru, G. Brănoiu, I. Ramadan, F. Miculescu, Degradation of automotive materials upon exposure to sunflower biodiesel, Ind. Crops Prod. 54 (Mar. 2014) 149–158.

[12] S. Kaul, et al., Corrosion behavior of biodiesel from seed oils of Indian origin on diesel engine parts, Fuel Process. Technol. 88 (3) (Mar. 2007) 303–307.

[13] K. Chew, A. Haseeb, H. Masjuki, M. Fazal, M. G.- Energy, and undefined, Corrosion of Magnesium and Aluminum in Palm Biodiesel: A Comparative Evaluation, Elsevier, 2013. Accessed: Feb. 15, 2018. [Online]. Available: https://www.sciencedirect.com/science/article/pii/S0360544213003824.

[14] E. Hu, Y. Xu, X. Hu, L. Pan, S. J.-R. energy, and undefined, Corrosion Behaviors of Metals in Biodiesel from Rapeseed Oil and Methanol, Elsevier, 2012. Accessed: Feb. 15, 2018. [Online]. Available: https://www.sciencedirect.com/science/article/pii/S0960148111003922.

[15] D. Geller, T. Adams, J. Goodrum, J. P.- Fuel, and undefined, Storage Stability of Poultry Fat and Diesel Fuel Mixtures: Specific Gravity and Viscosity, Elsevier, 2008. Accessed: Mar. 13, 2019. [Online]. Available: https://www.sciencedirect.com/science/article/pii/S0016236107001810.

[16] M. Sgroi, G. Bollito, G. Saracco, S. Specchia, BIOFEAT: biodiesel fuel processor for a vehicle fuel cell auxiliary power unit: study of the feed system, J. Power Sources 149 (Sep. 2005) 8–14.

[17] M.A. Fazal, A.S.M.A. Haseeb, H.H. Masjuki, Effect of temperature on the corrosion behavior of mild steel upon exposure to palm biodiesel, Energy 36 (5) (May 2011) 3328–3334.

[18] M. Fazal, M. Jakeria, A.H.-I.C. and Products, and undefined, Effect of Copper and Mild steel on the Stability of Palm Biodiesel Properties: A Comparative Study, Elsevier, 2014. Accessed: Jan. 18, 2019. [Online]. Available: https://www.sciencedirect.com/science/article/pii/S0926669014001538.

[19] "ASTM G1 - 90(1999)e1 Standard Practice for Preparing, Cleaning, and Evaluating Corrosion Test Specimens." https://www.astm.org/DATABASE.CART/HISTORICAL/G1-90R99E1.htm (accessed Jul. 16, 2019).

[20] "ASTM G31 - 72(2004) Standard Practice for Laboratory Immersion Corrosion Testing of Metals." https://www.astm.org/DATABASE.CART/HISTORICAL/G31-72R04.htm (accessed Jul. 16, 2019).

[21] "J1747: Recommended Methods for Conducting Corrosion Tests in Hydrocarbon Fuels or Their Surrogates and Their Mixtures with Oxygenated Additives - SAE International." https://www.sae.org/standards/content/j1747_201305/ (accessed Jul. 16, 2019).

[22] T. Tsuchiya, H. Shiotani, S. Goto, G. Sugiyama, A. Maeda, Japanese Standards for Diesel Fuel Containing 5% FAME: Investigation of Acid Generation in FAME Blended Diesel Fuels and its Impact on Corrosion, 2006. Accessed: Feb. 15, 2018. [Online]. Available: http://papers.sae.org/2006-01-3303/.

[23] M. Fazal, A. Haseeb, H.M.-F.P. Technology, and undefined, Effect of Different Corrosion Inhibitors on the Corrosion of Cast Iron in Palm Biodiesel, Elsevier, 2011. Accessed: Jul. 16, 2019. [Online]. Available: https://www.sciencedirect.com/science/article/pii/S0378382011002323.

[24] R.W. Robert, W. Revie and H.H. Uhlig, Corrosion and Corrosion Control: An Introduction to Corrosion Science and Engineering.

[25] M. Fazal, A. Haseeb, H.M.-F.P. Technology, and undefined, Comparative Corrosive Characteristics of Petroleum Diesel and Palm Biodiesel for Automotive Materials, Elsevier, 2010. Accessed: Feb. 15, 2018. [Online]. Available: https://www.sciencedirect.com/science/article/pii/S0378382010001293.

[26] S. Klimas, K. Fruzzetti, C. Turner, P. Balakrishnan, G. Strati, R. Tapping, Identification and testing of amines for steam generator corrosion and fouling control, Heat Exch. Fouling Clean. Fundam. Appl. (May 2003). Accessed: Feb. 15, 2018. [Online]. Available: http://dc.engconfintl.org/heatexchanger/37.

[27] R. Ávila, J.S.-I.C. and Products, and undefined, Physical-Chemical Properties and Thermal Behavior of Fodder Radish Crude Oil and Biodiesel, 2012 cabdirect.org, Accessed: Feb. 15, 2018. [Online]. Available: https://www.cabdirect.org/cabdirect/abstract/20123104831.

[28] L. Bellot-Gurlet, D. Neff, S. Reguer, J. M.-J. of N., and undefined, Raman studies of corrosion layers formed on archaeological irons in various media, Trans. Tech. Publ. (2009). Accessed: Feb. 16, 2018. [Online]. Available: https://www.scientific.net/JNanoR.8.147.

[29] G. Pingitore, T. Cerchiara, G. C.-J. of C., and undefined, Structural Characterization of Corrosion Product Layers on Archaeological Iron Artifacts from Vigna Nuova, Crotone (Italy), Elsevier, 2015. Accessed: Feb. 16, 2018. [Online]. Available: https://www.sciencedirect.com/science/article/pii/S1296207414001083.

[30] S. Das, M. H.-C. Geology, and undefined, Application of Raman Spectroscopy to Identify Iron Minerals Commonly Found in Mine Wastes, Elsevier, 2011. Accessed: Jul. 17, 2019. [Online]. Available: https://www.sciencedirect.com/science/article/pii/S0009254111003500.

[31] Q. Xu, K. Gao, Y. Wang, X. P.-A. S. Science, and undefined, Characterization of Corrosion Products Formed on Different Surfaces of Steel Exposed to Simulated Groundwater Solution, Elsevier, 2015. Accessed: Jul. 17, 2019. [Online]. Available: https://www.sciencedirect.com/science/article/pii/S0169433215007394.

[32] X. Kui, C. Dong, X. Li, F. W.-J. of I. and S. Research, and undefined, Corrosion Products and Formation Mechanism during Initial Stage of Atmospheric Corrosion of Carbon Steel, Elsevier, 2008. Accessed: Jan. 18, 2019. [Online]. Available: https://www.sciencedirect.com/science/article/pii/S1006706X08602472.

[33] A. Rajasekar, S. Maruthamuthu, N. Palaniswamy, A. Rajendran, Biodegradation of corrosion inhibitors and their influence on petroleum product pipeline, Microbiol. Res. 162 (4) (Sep. 2007) 355–368.

[34] D. Martínez, R. Gonzalez, K. Montemayor, A. Juarez-Hernandez, G. Fajardo, M.A.L. Hernandez-Rodriguez, Amine type inhibitor effect on corrosion–erosion wear in oil gas pipes, Wear 267 (1–4) (Jun. 2009) 255–258.

[35] M.A. Deyab, Adsorption and inhibition effect of ascorbyl palmitate on corrosion of carbon steel in ethanol blended gasoline containing water as a contaminant, Corros. Sci. 80 (Mar. 2014) 359–365.

[36] M. Bernard, S.J.-E. Acta, and undefined, Understanding Corrosion of Ancient Metals for the Conservation of Cultural Heritage, Elsevier, 2009. Accessed: Jan. 18, 2019. [Online]. Available: https://www.sciencedirect.com/science/article/pii/S0013468609000942.

[37] E. Mattei, G. de Vivo, A. De Santis, C. Gaetani, C. Pelosi, U. Santamaria, Raman spectroscopic analysis of azurite blackening, J. Raman Spectrosc. 39 (2) (Feb. 2008) 302–306.

[38] G. Smith, R.C.-J. of A. Science, and undefined, Raman Microscopy in Archaeological Science, Elsevier, 2004. Accessed: Jan. 18, 2019. [Online]. Available: https://www.sciencedirect.com/science/article/pii/S0305440304000238.

[39] M. Bouchard, D. S.-S. A. P. A. M. and, and undefined, Catalogue of 45 Reference Raman Spectra of Minerals Concerning Research in Art History or Archaeology, Especially on Corroded Metals and Coloured Glass, Elsevier, 2003. Accessed: Jan. 18, 2019. [Online]. Available: https://www.sciencedirect.com/science/article/pii/S1386142503000696.